Revision 2

Word count: 8163

On the crystal chemistry of sulfur-rich lazurite, ideally $Na_7Ca(Al_6Si_6O_{24})(SO_4)(S_3)^{-}\cdot nH_2O$

ANATOLY N. SAPOZHNIKOV[1], VLADIMIR L. TAUSON[1], SERGEI V. LIPKO[1], ROMAN YU. SHENDRIK[1], VALERY I. LEVITSKII[1], LYUDMILA F. SUVOROVA[1], NIKITA V. CHUKANOV[2], MARINA F. VIGASINA[3]

[1]Vinogradov Institute of Geochemistry, Siberian Branch of Russian Academy of Sciences, 1a Favorsii St., Irkutsk, 664033, Russia

[2]Institute of Problems of Chemical Physics, Russian Academy of Sciences, Chernogolovka, Moscow region, 142432, Russia

[3]Faculty of Geology, Moscow State University, Vorobievy Gory, 119991 Moscow, Russia

ABSTRACT

Dark blue lazurite from the Malo-Bystrinskoe lazurite deposit, Baikal Lake area, Eastern Siberian region, Russia was analysed by electron microprobe and revealed an unusually high content of total sulfur corresponding to 8.3 wt% S. The relative content of sulfur in sulfate and sulfur in sulfide form was determined by wet chemical analysis. The H_2O content was measured by means of differential thermal analysis in combination with mass spectrometry and infrared (IR) spectroscopy. The charge-balanced empirical formula of lazurite calculated on the basis of 12 (Al+Si) atoms per formula unit was $(Na_{6.97}Ca_{0.88}K_{0.10})_{\Sigma 7.96}[(Al_{5.96}Si_{6.04})_{\Sigma 12}O_{24}](SO_4)^{2-}_{1.09}(S_3^{-})_{0.55}S^{2-}_{0.05}Cl_{0.04}\cdot 0.72H_2O$. The presence of H_2O molecules and $(S_3)^{-}$ and $(SO_4)^{2-}$ groups was confirmed by the combination of IR, Raman, electron paramagnetic resonance (EPR), and X-ray photoelectron spectroscopy (XPS) methods. The idealized formula of lazurite is $Na_7Ca[Al_6Si_6O_{24}](SO_4)^{2-}(S_3)^{-}\cdot H_2O$, and it is believed that extra-framework cations and anions are grouped into clusters of $[Na_3Ca\cdot SO_4]^{3+}$ and $[Na_4(S_3)^{-}]^{3+}$. The types of isomorphous

substitutions in nosean and haüyne are discussed. Lazurite is a clathrate-type mineral, which may be an effective $(S_3)^-$ sensor due to the stability of the trisulfur radical anion in isolated cages of the crystal structure. This specific feature makes it possible to study the behavior of this ubiquitous radical anion over larger *T* and *P* ranges as compared to free species. This kind of lazurite, with oxidized and reduced sulfur species, seems to be appropriate for the estimation of the fugacity of SO_2 and O_2 in metasomatic systems forming lazurite-containing rocks. The systematic presence of incommensurate modulations is a unique structural feature of Baikal lazurite and may be an important marker indicating provenance of the mineral.

Keywords: Microporous mineral structure, lazurite, sulfide radical ion, X-ray diffraction, spectroscopy, superstructure

INTRODUCTION

The mineral lazurite belongs to the large family of feldspathoids (so-called cancrinite-sodalite family) whose frameworks contain six-membered rings of Si- and Al-centered tetrahedra. These rings form different strata denoted by the letters A, B, and C. Every ring is linked to three rings of the preceding layer and to three rings of the succeeding layer. The stacking sequence of the *A*, *B*, *C* layers determines the topological type of framework. Minerals and synthetic materials with sodalite-type framework topology (the ABC_∞ stacking sequence) are characterized by specific microporous structures with so-called sodalite cages (β-cages) hosting different cations, anions, and neutral molecules. In the current International Mineralogical Association (IMA) list of minerals, the idealized formula of lazurite is given as $Na_3Ca(Si_3Al_3)O_{12}S$.

Lazurite is one of the main components of the rock lapis lazuli which has long attracted attention as a beautiful ornamental gemstone. Well known are ancient lazurite artifacts, such as

vases, boxes, statues, amulets, and carved art products. The State Hermitage Museum (St. Petersburg, Russia) exhibits lazurite-lined countertops and a vase carved from a monolithic stone. In addition to using the material for stone-cutting products and jewellery, lazurite powder was used in painting. Renaissance artists produced ultramarine, an excellent blue paint prepared from the powder of the "heavenly stone," wax, and oil. The paint did not fade in the sun and was not damaged by dampness or fire. Ultramarine was used to paint the blue sky, the blue sea, and even the robe of the Virgin Mary. It was applied by Raphael, Leonardo da Vinci, Michelangelo, and many other painters. The paint was considered indispensable, not only for painting, but also in dyeing expensive clothes (Ivanov and Sapozhnikov 1985; Gadiyatov 2012).

It was supposed that the blue color of the stone is associated with molecular radical ions $(S_3)^-$ and $(SO_4)^-$ within its structure (Samoilovich 1971). Most researchers have accepted the relationship between the blue color of lazurite and the radical ion $(S_3)^-$ as an indisputable fact (Platonov et al. 1971). Nevertheless, it has been noted that sulfur is present mainly in the form of sulfate in both synthesized and natural S-bearing blue sodalite-type compounds, with the polysulfides concentrated below the detection limit of X-ray absorption near-edge spectroscopy (XANES) and XPS methods (Fleet et al. 2005). According to the EPR data, the color centers observed in lazurite and ultramarine have a “hole” nature, in other words, they form by the loss of an electron (Samoilovich 1971; Ostroumov et al. 2002).

Lazurite is one of the three cubic sulfate-containing minerals of the sodalite group, and according to the accepted idealized formula of lazurite given in the IMA list of minerals, lazurite is a sodalite-type aluminosilicate with sulfide sulfur prevailing among extra-framework anions. The structure of sodalite-type aluminosilicate minerals is based on the framework $[Al_6Si_6O_{24}]^{6-}$, in large cavities of which occur cations Na^+, Ca^{2+}, and K^+ that compensate the charge of the framework, and additional anions Cl^-, $(SO_4)^{2-}$, S^{2-}, and $(OH)^-$. Extra-framework cations and

This is the peer-reviewed, final accepted version for American Mineralogist, published by the Mineralogical Society of America.
The published version is subject to change. Cite as Authors (Year) Title. American Mineralogist, in press.
DOI: https://doi.org/10.2138/am-2020-7317. http://www.minsocam.org/

anions form clusters, the composition, size, and charge of which determines the originality of the structure of each particular mineral (Hassan and Grundy 1984, 1989, 1991; see Table 1).

Table 1. Formulas of minerals of the sodalite group, the cluster occupancy of the sodalite cages, and values of the unit cell parameter (*a*).

Mineral	**Formula**	**Occupation (%)**	***a*** **(Å)**	**Reference**
Sodalite	$Na_8[Al_6Si_6O_{24}]Cl_2$	$100[Na_3 \cdot Cl]^{3+}$	8.882(1)	Hassan and Grundy 1984
Nosean	$Na_8[Al_6Si_6O_{24}](SO_4) \cdot H_2O$	$50[Na_4 \cdot SO_4]^{2+}$ $50[Na_4 \cdot H_2O]^{4+}$	9.084(2)	Hassan and Grundy 1989
Haüyne	$Na_{4.5}Ca_2K[Al_6Si_6O_{24}](SO_4)_{1.5}(OH)_{0.5}$	$75[Na_3Ca \cdot SO_4]^{3+}$ $25[K_2Ca \cdot OH]^{3+}$	9.116(1)	Hassan and Grundy 1991
Lazurite	$Na_6Ca_2[Al_6Si_6O_{24}](SO_4)_{1.4}S_{0.6}$	$71[Na_3Ca \cdot SO_4]^{3+}$ $29[Na_3Ca \cdot S]^{3+}$	9.105(2)	Hassan et al. 1985

Note: Mineral structures are determined within the space group $P\bar{4}3n$. However, it is accepted that real sulfate-containing mineral structures consist of two types of domains either of which has ordered structure and symmetry of P23 reduced against the space group $P\bar{4}3n$ (Hassan and Grundy 1989).

It should be added that the optically anisotropic rhombic lazurite

$Na_{6.4}Ca_{1.5}[Si_6Al_6]_{12}O_{24}(SO_4)_{1.6}(S_3)^-_{0.2} \cdot 0.62H_2O$, space group Pnaa, a = 9.066(2), b = 12.851(2), c = 38.558(4), Z = 6, is approved by IMA (No. 2010-070) as the mineral vladimirivanovite (Sapozhnikov et al. 2012). It has a dark-blue color, and its framework is topologically identical to the frameworks of minerals of the sodalite group, although the unit cell is six times larger than the unit cell of cubic lazurite. It is noteworthy that the charge balance in the vladimirivanovite formula can be achieved only on condition that sulfide sulfur forms radical anion $(S_3)^-$.

As noted earlier, the ideal formula of lazurite is $Na_6Ca_2[Al_6Si_6O_{24}]S_2$, where S is the S^{2-} anion. However, Hassan et al. (1985) were unable to explain the amount of sulfur, often exceeding 2 atoms per formula unit, which may violate the electroneutrality of the formula. To solve this problem, Hogarth and Griffin (1976) proposed that excess sulfur occurs within the framework, partially replacing oxygen atoms.

Taylor (1967) measured the superstructural periodicity of nine sulfate-enriched sodalites and found their superstructure to be incommensurate according to the satellite reflections in the X-ray diffraction (XRD) patterns. In nosean, haüyne, and lazurite containing tetrahedral anions of $(SO_4)^{2-}$, the ordering of clusters of different sizes causes modulation of the displacement of the oxygen atoms in the framework, resulting in superstructural reflections appearing in diffraction patterns (Hassan and Buseck 1989). In non-cubic varieties of lazurite, the commensurate superstructure can be caused by modulation of the displacement of AlO_4 and SiO_4 tetrahedra from their positions in the cubic mineral (Evsyunin et al. 1997, 1998). Commensurability or incommensurability of the superstructure is estimated by the value of the satellite displacement from the main reflection along the axis of the reciprocal lattice. If the displacement fits between the main reflections an integer number of times, the superstructure is commensurate; otherwise, it is incommensurate. Satellite displacement (structure modulation parameter) may be different in different samples. In optically isotropic cubic lazurite samples, the value of the incommensurate modulation parameter varies from 0.169 to 0.217 (Sapozhnikov 1992). According to Bolotina (2006), incommensurate modulation in lazurite is due to the alternation of three-dimensional areas of diverse volumes in its structure.

The aim of this work was to study the properties and chemical composition and to specify the crystal-chemical formula of S-rich lazurite using a combination of mineralogical, chemical, and physical analytical methods. In the study, two samples (Fig. 1) of dark blue lazurite with high sulfur contents were collected from the Malo-Bystrinskoe lazurite deposit (Baikal Lake

area, Russia). The samples are structurally unique among lazurites from different locations and differ from them by the incommensurate modulation parameter equal to 0.147.

GEOLOGICAL SETTING AND PETROLOGICAL DATA

Rocks with high-sulfur lazurite are lenticular metasomatic bodies ranging in size from 4 cm × 7 cm to 15 cm × 30 cm (sample 1) and lazurite-containing calciphyres (sample 2). In sample 1, the lazurite contained varying amounts of subordinate forsterite, pyroxene, and calcite. This type of rock is rare for the Malo-Bystrinskoe deposit. The second sample was lazurite-containing calciphyre with minor bystrite. Both rocks were confined to dolomite marbles.

The lazurite-dominant rocks (sample 1) have a taxitic structure due to the irregular accretion of dark blue lazurite among white calcite, diopside, forsterite, and rare phlogopite. Lazurite aggregates were composed of dark blue single-crystal individuals ranging in size from 0.2 to 5 mm with perfect cleavage. The mineral content (wt%) in the rock was: phlogopite, up to 10; forsterite, 5–20; pyroxene, 5–30; calcite 40–60; and lazurite 60–95. This type of rock is an apocarbonate lazurite metasomatite, developed within early forsterite, pyroxene, and forsterite-pyroxene skarns of the magmatic stage. This was evidenced by observations in thin sections: grains of forsterite and pyroxene were corroded by lazurite and phlogopite and were present as relics of different shapes in poikiloblasts of lazurite; moreover, some lazurite crystals formed as a result of recrystallization and do not contain inclusions. Small relic grains of dolomite are dispersed randomly in calcite aggregates in amounts up to 3 wt%. In addition, grains of corroded pyrite were observed in lazurite-bearing metasomatic rocks. The early generation of calcite is represented by individual grains (0–7%) represented by calcite syngenetic with lazurite which forms coarse crystals and irregular scalloped edges of granules. Lazurite, in addition to forsterite and diopside inclusions, may contain early skeletal (graphic, diablast) pyroxene-lazurite accretions 2–6 mm in size.

Polycrystalline aggregates of lazurite can reach several centimeters across and, as a rule, are the later products of early lazurite recrystallization. In general, the dominating metasomatic structure is heterogranoblastic, with areas of microdiablastic structures containing varying amounts of diopside, forsterite, calcite, and lazurite in the form of individual grains and their intergrowths.

The second type of rock (sample 2) is represented by lazurite-containing calciphyres, dominated by calcite (70–80%). Forsterite and pyroxene (5–10% each), lazurite (10–15%), bystrite (1–3%), and minor phlogopite are also present. These rocks are characterized by a very irregular distribution of silicates and aluminosilicate minerals, including lazurite. Bystrite occurs in lazurite-containing calciphyres as pseudomorphs after lazurite grains.

In transmitted light, both samples of S-rich lazurite have a saturated dark blue color with different shades that is virtually uniform within each individual sector. Their "velvet" color differs from the usual blue color of lazurite with deeper intensity. Observations in cross-polarized light (in crossed nicols) in one-third of the cases demonstrated near complete extinction with dark brown tints. The absence of complete extinction indicates slightly non-isotropic optical properties. In some cases, abnormal color with dark gray shades was observed in cross-polarized light.

It should be noted that the X-ray diffraction patterns of samples 1 and 2 near the lines of lazurite showed weak lines of sodalite, although sodalite was not observed in the thin section. However, the presence of sodalite forming thin zones (up to 10 μm) around lazurite grains as well as in cracks in lazurite (together with calcite) was detected by characteristic X-ray radiation of Cl. It is evident that the surficial substitution of lazurite by sodalite occurred under the action of late fluid deficient in sulfur and enriched in NaCl.

The rocks studied formed after the carbonate substrate, in some areas with complete replacement of early diopside-forsterite-containing metasomatites. This differs from the usual

way of formation after alumosilicate (granite, syenite, nepheline syenite) substrates. In thin sections of both rock types with high-S lazurite, we observed net-like (graphic) lazurite structures in calcite, as well as replacement of forsterite and diopside by lazurite and formation of diablastic intergrowths of diopside with lazurite in the carbonate substrate.

METHODS OF STUDY

Chemical composition

The samples of lazurite were studied on a JXA_8200 Jeol electron microprobe equipped with a high-resolution scanning electron microscope, an energy dispersion system (EDS), a SiLi detector with a resolution of 133 eV, and five wave dispersion spectrometers (WDS). The chemical composition was measured with WDS operated at an acceleration voltage of 20 kV, with a current intensity of 10 nA and a counting time of 10 s. The beam was defocused to 20 μm to decrease the thermal effect on the sample. Under these conditions, the mineral was stable with respect to the beam effect.

The following standards and analytical lines were used: pyrope (Si, Kα), albite (Al, Na, Kα), diopside (Ca, Kα), orthoclase (K, Kα), barite (S, Kα), and Cl-apatite (Cl, Kα). The contents of the elements were calculated using the ZAF procedure. Quantitative analyses of 30 local areas in sample 1 and 30 local areas in sample 2 were conducted. The compositions of six grains were measured for each sample; the intensities of analytical lines were measured at five points in each grain. The relative standard deviation characterizing reproducibility of the measurement of the determined element and chemical homogeneity of the samples did not exceed 1.3% for Al and Si; 2% for Na, S, and Ca; or 3% for Cl and K, which indicates the regular distribution of mineral-forming elements in lazurite. The back-scattered images obtained by scanning sample areas did not reveal sulfide inclusions (FeS_2, FeS).

Electron microprobe analysis (EMPA) was used to determine the total sulfur content in the samples. Sulfate sulfur in sample 1 was determined by conventional wet chemical analysis

using acidic decomposition. Sulfide sulfur was accepted as the difference between the total sulfur and the sulfate sulfur.

Thermoanalytical study

Thermal analysis was performed on a synchronous thermal analyser (STA 449 F1 Jupiter). Control of the composition of the gaseous thermolysis products was carried out using a quadrupole mass spectrometer (QMS 403 C Aëolos), with the energy of electron impact set at 70 eV. Over the course of sample heating, the tool enables simultaneous acquisition of data regarding changes in the sample weight, the rate of weight change, the thermal effects in the system, and the composition of the released gaseous phase. The thermal data were obtained in an argon atmosphere, in the temperature range from 20 to 1400 ºC, at a heating rate of 5 ºC/min.

Spectroscopic study

The infrared absorption spectra of high-S lazurite were measured by Fourier-transform IR spectroscopy (FTIR) using an FT-801 (Simex, Russia) and ALPHA FTIR spectrometer (Bruker Optics). Powdered samples were mixed with anhydrous KBr, pelletized, and analyzed at a resolution of 4 cm^{-1}. A total of 16 scans were collected in the wavenumber range 360 to 3800 cm^{-1}. The IR spectrum of an analogous pellet of pure KBr was used as a reference.

Lazurite dehydration was conducted as follows. Lazurite and KBr were ground in a mortar, kept at a given temperature for 10 min in a muffle furnace, and then cooled to room temperature. Thereafter, two tablets were pressed, one from a mixture of lazurite and KBr and another one (reference sample) from pure KBr. The IR spectrum of the latter was subtracted from the spectrum of the sample with lazurite. Next, powders of both samples were heated to the next temperature in the interval from 25–600 °C, and the procedure was repeated. Tablets were prepared and absorption spectra were measured under conditions of low relative humidity (< 20%); therefore, water adsorption in heated samples can be neglected.

The Raman spectrum of a randomly oriented S-rich lazurite sample was obtained using an EnSpectr R532 spectrometer based on an OLYMPUS CX 41 microscope coupled with a diode laser (λ = 532 nm) at room temperature. The spectrum was recorded in the range of 100 to 4000 cm^{-1} with a diffraction grating of 1800 gr mm^{-1} and a spectral resolution of 6 cm^{-1}. The output power of the laser beam was 5 mW. The diameter of the focal spot on the sample was less than 5 μm. The backscattered Raman signal was collected with a 40x objective; signal acquisition time for a single scan of the spectral range was 1 s, and the signal was averaged over 50 scans. Crystalline silicon was used as the standard.

The EPR experiment was performed on the lazurite using an X-band spectrometer RE1306 operated at a microwave frequency of 9380 MHz. The spectrometer was equipped with a cryostat operated at temperatures down to 77 K.

The XPS spectra were obtained with a SPECS instrument (SPECS, Germany) equipped with a PHOIBOS 150 MCD-9 hemispherical electron energy analyzer. The spectra were acquired at excitation initiated by monochromated AlKα (1486.74 eV) radiation with a power of 220 W and voltage at the tube of 12.5 kV. The high-resolution spectrum of S 2p (narrow scan) was recorded with a 0.05 eV interval and transmission energy of 8 eV. Lazurite sample 1 was powdered to a mean particle size of 0.01–0.02 mm immediately before placing it in the analysis chamber. The surface of the sample was not purified by ion etching. This is important in the study of lazurite because etching by Ar^+ causes a reduction of sulfate sulfur. The C 1s peak at 285 eV from natural hydrocarbon contaminants was used to correct the binding energies (BE) for the surface charging. The 2p sulfur spin-orbital doublet was unfolded and fitted by CasaXPS software after subtracting the nonlinear background by Shirley's method and taking into account separation of the doublet components S $2p_{3/2}$ and S $2p_{1/2}$ equal to 1.2 eV and the proportion of their intensities as 2:1. The peak shapes were described by the Voigt function (i.e., convolution

of Gauss and Lorentz functions). Peak attribution was performed according to data published previously (Tauson et al. 2012). The accuracy of the BE was estimated to be ± 0.1 eV.

X-ray diffraction study

The X-ray diffraction study was carried out by the photo method on a single crystal (RKV-86 camera, $CuK_{\alpha+\beta}$ radiation) and the powder diffraction method with an automatic powder diffractometer (D8 ADVANCE, Bruker, Germany) equipped with a Göbel mirror. The powder X-ray diffraction patterns were obtained in step scan mode (in the 2θ range of 5 to 70°), using CuKα radiation, at an accelerating voltage of 40 kV, current of 40 mA, time per step of 1 s, and 2θ step of 0.02°. The calculations of interplanar distances and intensities of diffraction lines were performed using the computational software that was delivered with the diffractometer (DIFFRAC Plus Evaluation package EVA, Bruker AXS). The description of the modulated structure was carried out using a previously published scheme (Sapozhnikov 1992) with the modulation parameter estimated in the present work. The dependence of the unit cell parameter on temperature for a sample heated up to 750 °C in air was calculated based on the position of the 440 line, which was measured in situ in the course of heating a sample placed on the camera of the diffractometer using a high-temperature cell NTK 16.

RESULTS AND DISCUSSION

Chemical composition and formula of lazurite

According to the electron microprobe analyses (Table 2), the total content of sulfur in the S-rich lazurite (sample 1) was 8.30 wt%. According to the wet chemistry studies performed, the mineral contained sulfate sulfur in the amount of 3.23 wt% S^{6+} which corresponds to 8.08 wt% SO_3. The amount of sulfide sulfur was calculated as the difference between total sulfur and sulfate sulfur and was equal to 5.07 wt%.

Table 2. Chemical composition of high-sulfur lazurite (samples 1 and 2) and stoichiometric coefficients for the components calculated on (Al + Si) = 12 atoms per formula unit.

This is the peer-reviewed, final accepted version for American Mineralogist, published by the Mineralogical Society of America.
The published version is subject to change. Cite as Authors (Year) Title. American Mineralogist, in press.
DOI: https://doi.org/10.2138/am-2020-7317. http://www.minsocam.org/

Component	Mean content		Range		Atom /group	Formula coefficient	
	1	2	1	2		1	2
SiO_2	33.48	33.15	34.33–32.35	33.64–31.64	Si	6.04	6.01
Al_2O_3	28.02	28.06	28.33–27.64	28.70–27.41	Al	5.96	5.99
CaO	4.56	4.35	4.79–4.13	4.94–4.22	Ca	0.88	0.85
Na_2O	19.94	20.27	20.57–19.00	20.98–18.72	Na	6.97	7.12
K_2O	0.43	0.04	0.53–0.31	0.10–0.02	K	0.10	0.01
Cl	0.13	0.02	0.21–0.07	0.06–0.01	Cl	0.04	0.02
SO_3	8.08*	7.35***			SO_4	1.09	1.00***
S	5.07**	7.23**			S_3	0.55	0.82***
					S	0.05	-
H_2O	1.2	n.d.			H_2O	0.72	n.d.
–O=S	–0.42	–0.60					
–O=Cl	–0.03	0					
Total	**100.46**	**99.87**					

n.d. not determined
–O=S is calculated for $(S_3)^-$
*Determined by wet chemical analysis
**Calculated as the difference between total sulfur and sulfate sulfur
***Calculated based on the charge-balance condition; all sulfide sulfur in sample 2 was considered $(S_3)^-$

The empirical formula based on 12 (Si+Al) atoms per formula unit under the assumption that all sulfide sulfur is present in the form of S^{2-} (in accordance with the standard lazurite formula given in the IMA list of minerals) is $(Na_{6.97}Ca_{0.88}K_{0.10})_{7.95}[Al_{5.96}Si_{6.04}]_{12}O_{24}(SO_4)_{1.09}(S^{2-})_{1.71}Cl_{0.04}\cdot 0.72H_2O$. This formula is unbalanced in charge, with the sums of cations and anions equal to +50.87 and –53.64 charge units, respectively. However, sulfur atoms are known to be present in the structure of lazurite in the form of radical ions, such as $(S_2)^-$ and $(S_3)^-$ (Platonov et al. 1971; Clark et al. 1983; Gobeltz-Hautecoeur et al. 2002). To achieve electroneutrality, 1.71 sulfide sulfur atoms should be combined into groups with a total charge of –0.65. This is possible only under the assumption that part of the sulfide sulfur belongs to the trisulfide radical anion

because all other variants result in excess negative charge. On the other hand, the assumption that $(S_3)^-$ is the only form of sulfide sulfur in S-rich lazurite leads to a deficit of negative charge.

Table 3 shows different variants of combining sulfide sulfur atoms, which result in electroneutrality of the empirical formula. All combinations resulted in a significant dominance of the trisulfide radical anion over other forms of sulfide sulfur. Despite the fact that all combinations given in Table 3 agree with the chemical data and the charge balance requirement, only variant no. 1 is acceptable because Raman and XPS data exclude all sulfide anions except $(S_3)^-$ and S^{2-} (Table 3).

Table 3. Different variants incorporating 1.7 atoms of sulfide sulfur into the lazurite structure under the assumption that the total charge is equal to –0.65

Variant no.	Amount of different sulfide ions	Charge of formula
1	$(S_3)^-_{0.55} + (S^{2-})_{0.05}$	–0.65
2	$(S_3)^-_{0.53} + (S_2)^{2-}_{0.06}$	–0.65
3	$(S_3)^-_{0.49} + (S_3)^{2-}_{0.08}$	–0.65
4	$(S_3)^-_{0.41} + (S_2)^-_{0.24}$	–0.65

Samples 1 and 2 have similar contents of most components (Table 2), but differ in total sulfur content (8.30 wt% in sample 1 and 10.17 wt% in sample 2). Unfortunately, we were unable to determine the amount of sulfate sulfur in sample 2 by chemical methods due to the lack of pure material. Calculation of the formula under the assumption that the number of Ca atoms is equal to the number of SO_4 groups (in accordance with crystal-chemical considerations, see below), showed that $(S_3)^-$ is the predominant form of sulfur in sample 2 (Table 2). The mineral contained more sulfide than sulfate sulfur, which is a distinctive feature among lazurites from the Baikal Lake area.

The formulas of the samples were balanced in charge, emphasizing the fact that sulfide sulfur in lazurite was represented mainly by the radical ion $(S_3)^-$, the presence of which is in

agreement with the dark blue color of the mineral and confirms the conclusion that "the connection of the blue color (of lazurites) with the radical $(S_3)^-$ is … an indisputable fact" (Platonov et al. 1971).

The ideal chemical formula for S-rich lazurite is $Na_7Ca[Al_6Si_6O_{24}]SO_4(S_3)^-\cdot H_2O$, and in comparison with the idealized formula of nosean—$Na_8[Al_6Si_6O_{24}]SO_4\cdot H_2O$–and haüyne—$(Na,K)_6Ca_2[Al_6Si_6O_{24}](SO_4)_2$—reveals the difference in the charge value of the extra-framework cations. In nosean, it equals +8. In the mineral under study, it equals +9, and in haüyne, it is +10 charge units. It should be noted that sulfate-free lazurite with the idealized formula—$Na_6Ca_2[Al_6Si_6O_{24}](S^{2-})_2$—has not been found in nature. However, Tauson et al. (1998) synthesized such a compound, so-called "S-sodalite," as a product of annealing of lazurite at 800 °C and low fugacity of SO_2 in the gaseous phase. This compound has gray color and a unit-cell parameter of 8.944 Å, which is close to the *a* parameter of sodalite (Table 1).

Thermal analysis

A comparison of thermogravimetric (TG) and differential scanning calorimetry (DSC) data (Fig. 2) with ion currents corresponding to different mass numbers led us to conclude that endothermic effects observed in the temperature ranges 300–550 (I), 550–670 (II), 960–1300 (III), and 1300–1450 °C (IV) and accompanied by a 1.2, 3.1, 11.4, and 3.5% weight loss were due to the release of H_2O (I), CO_2 (II) and SO_2 (III and IV) as a result of oxidation of sulfide groups (III), and SO_2 evolved from sulfate groups (IV), respectively.

Raman spectroscopy

Raman spectroscopy is a sensitive tool used to detect trisulfide anion radicals because Raman bands characteristic of S_3^- are strong (Climent-Pascual et al. 2009). Figure 3 shows the Raman spectrum of S-rich lazurite. Raman shifts (cm^{-1}), band intensities (s for strong, m for medium and w for weak), and assignment of bands are shown in Table 4.

Table 4. Raman spectrum characteristics of S-rich lazurite

This is the peer-reviewed, final accepted version for American Mineralogist, published by the Mineralogical Society of America.
The published version is subject to change. Cite as Authors (Year) Title. American Mineralogist, in press.
DOI: https://doi.org/10.2138/am-2020-7317. http://www.minsocam.org/

Raman shift (cm^{-1})	Intensity	Assignment of bands
257	m	ν_2 (A_2) of S_3^- – bending vibrations
285	w	combination of lattice modes
546	s	ν_1 (A_1) of S_3^- – stretching vibrations
585	m	ν_4 of SO_4^{2-} – bending vibrations
811	w	combination mode $\nu_{1+}\nu_2$ of S_3^-
988	w	ν_2 of SO_4^{2-} – symmetric stretching vibrations
1093	s	overtone $2\nu_1$ of S_3^-
1363	w	combination mode $2\nu_{1+}\nu_2$ of S_3^-
1638	m	overtone $3\nu_1$ of S_3^-
1903	w	combination mode $3\nu_{1+}\nu_2$ of S_3^-
2181	w	overtone $4\nu_1$ of S_3^-
2440	w	combination mode $4\nu_{1+}\nu_2$ of S_3^-
2720	w	overtone $5\nu_1$ of S_3^-

The assignment of bands was made in accordance with Reshetnyak et al. (1986), Steudel (2003), Tossell (2012), and Chivers and Elder (2013).

It is important to note that S^{2-} is the only sulfide anion that does not have internal vibrations. Bands of other sulfide anions, except those of S_3^-, were absent in the Raman spectrum of S-rich lazurite. This fact confirms the conclusion that only three kinds of S-bearing anions were present in sample 1: S_3^-, S^{2-}, and $(SO_4)^{2-}$.

Infrared spectroscopy

The strongest bands in the IR spectrum of S-rich lazurite (Fig. 4) were observed at 1000 cm^{-1} and in the ranges of 600–720 and 380–500 cm^{-1} which correspond to stretching, mixed, and bending modes of the tetrahedral framework, respectively. The band at 3420 cm^{-1} is due to O–H

337 stretching vibrations of H_2O molecules. Two bands of nondegenerate bending vibrations of H_2O
338 (at 1622 and 1683 cm^{-1}) indicate the presence of two kinds of locally non-equivalent water
339 molecules in the β-cages of S-rich lazurite. The band at 2342 cm^{-1} corresponds to antisymmetric
340 stretching vibrations of admixed CO_2 molecules (Bellatreccia et al., 2009; Balassone et al.,
341 2012).

342 As compared with the IR spectra of haüyne and nosean, the spectrum of S-rich lazurite is
343 characterized by lowered intensities in the bands of asymmetric S–O stretching vibrations of
344 $(SO_4)^{2-}$ anions (in the range 1090–1150 cm^{-1}) and the presence of an additional band at 580 cm^{-1}
345 associated with antisymmetric stretching vibrations in $(S_3)^-$ anions (ν_3 mode: Clark and Cobbold
346 1978; Wong 2003; Li et al. 2011; Chivers and Elder 2013) which confirms the content of $(S_3)^-$
347 anions in the sample. Climent-Pascual et al. (2009) suggested that $(S_3)^-$ anions can occupy up to
348 15% of the β-cages in the mineral structure.

349 Figure 5 shows the temperature dependence of the absorption band intensity in the region
350 of 3400 cm^{-1} which was obtained by measuring the optical density corresponding to the
351 absorption maximum; absorbance at 3200 cm^{-1} was used as background. The absorption of
352 lazurite, which was not subjected to thermal treatment, was accepted as equal to one. The most
353 intense release of H_2O was observed in the temperature range of 350–550 °C. Absorption spectra
354 in the IR region show that the lazurite samples were close to the previously synthesized
355 ultramarine-type lazurites (Arieli et al. 1992; Gesing 1998; Fechtelkord 1999; Climent-Pascual et
356 al. 2009).

357 **EPR spectroscopy**

358 The EPR spectrum of S-rich lazurite is shown in Figure 6. One broad line was observed
359 at $g = 2.030$. This signal was previously associated with the $(S_3)^-$ radical anion (Pinon et al.
360 1992). The g factor of $(S_3)^-$ is greater than that of a free electron, which corresponds to the model
361 of the $(S_3)^{-*}$ center with an electron and a hole on the outer shell of the anion.

This is the peer-reviewed, final accepted version for American Mineralogist, published by the Mineralogical Society of America.
The published version is subject to change. Cite as Authors (Year) Title. American Mineralogist, in press.
DOI: https://doi.org/10.2138/am-2020-7317. http://www.minsocam.org/

X-ray diffraction

The X-ray diffraction patterns of sample 1 contain basic and superstructural reflections (Table 5). Basic reflections define the primary cubic sub-cell with the parameter 9.087(3) Å and space group $P\bar{4}3n$.

Table 5. Powder X-ray diffraction data of high-sulfur lazurite (sample 1).

hkl*	$D_{meas.}$	$D_{calc.}$	***I***		***hkl****	$D_{meas.}$	$D_{calc.}$	***I***
110	6.437	6.426	18.4		1+*n*,1+*n*,4	2.111	2.105	3.7
2-0.5,1-0.5,1	4.867	4.857	6.7		4+*n*,1-*n*,1	2.091	2.089	5.8
200	4.548	4.544	8.3		4+*n*,1+*n*,1	2.057	2.057	3.3
210	4.067	4.064	4.7		4+0.5,1-0.5,1	1.9604	1.9598	3
2-*n*,1-*n*,1	4.009	4.001	4.5		332	1.9367	1.9374	3.7
1-*n*,1-*n*,2	3.895	3.891	4.4		3+*n*,2+*n*,3	1.8736	1.8739	3
211	3.711	3.710	100		2+*n*,2-*n*,4	1.8543	1.8533	2.7
1+*n*,1+*n*,2	3.530	3.528	5.3		510	1.7821	1.7822	9.4
2+*n*,1+*n*,1	3.450	3.453	4.6		4+*n*,1+*n*,3	1.7329	1.7323	2.6
220	3.211	3.213	4.3		3+0.5,3+0.5,2	1.7013	1.7022	2.5
2-0.5,1+0.5,1	3.117	3.117	7.3		521	1.6592	1.6591	3.4
2+0.5,1+0.5,1	2.948	2.948	4.7		4-*n*,0+*n*,4	1.6355	1.6357	2.6
310	2.875	2.874	16.3		440	1.6063	1.6064	7.2
2-*n*,2-*n*,2	2.761	2.757	4.8		433	1.5585	1.5585	4.2
222	2.623	2.623	29.5		442	1.5144	1.5146	3.8
3-*n*,2-*n*,1	2.564	2.563	4.2		532	1.4744	1.4742	4.8
2+*n*,2+*n*,2	2.499	2.499	4.5		6+*n*,0+*n*,2	1.4027	1.4054	2
321	2.428	2.429	7		6-*n*,2+*n*,2	1.3879	1.3880	2.1
3+*n*,1-*n*,2	2.372	2.376	3.9		622	1.3702	1.3700	5.6
2+*n*,1+*n*,3	2.349	2.352	3.4		631	1.3399	1.3399	2.4
3+*n*,2+*n*,1	2.308	2.307	3.6		444	1.3116	1.3116	3.8
400	2.272	2.272	8.3		550	1.2855	1.2851	2.5
4-*n*,1-*n*,1	2.236	2.232	4.1		5+2*n*,5-2*n*,0	1.2827	1.2829	2.3
4-*n*,1+*n*,1	2.194	2.194	3.7		5+*n*,0+*n*,5	1.2655	1.2661	1.9
411	2.142	2.142	15.7		721	1.2369	1.2366	3.8

*Simple symbols (110, etc.) denote the indices of basic reflections; symbols containing ±0.5 (2-0.5,1-0.5,1, *etc*.) refer to the powder diffraction lines of commensurate superstructure; symbols (*h*±*n*,*k*±*n*,*l*)—containing *n*, the parameter of the incommensurate modulation—refer to the lines of incommensurate superstructure (satellite reflections).

This is the peer-reviewed, final accepted version for American Mineralogist, published by the Mineralogical Society of America.
The published version is subject to change. Cite as Authors (Year) Title. American Mineralogist, in press.
DOI: https://doi.org/10.2138/am-2020-7317. http://www.minsocam.org/

371 Note: the sub-cell parameter a = 9.087(3) Å and n = 0.147.

372 Superstructural reflections of two types correspond to the commensurate and
373 incommensurate superstructure (Fig. 7). No reflections of admixed sodalite were observed in the
374 single-crystal X-ray rotation photographs. The [100] X-ray rotation photograph of a crystal (Fig.
375 8) demonstrated a small number of reflections of commensurate superstructure lying in the
376 middle of the basic reflection arrays (these reflections correspond to the lines at 4.867, 3.117,
377 2.948, 1.9604, and 1.7013 Å in Table 5). The incommensurate superstructure is registered by the
378 position of the satellites of the main reflections. Numerous satellites of the first order on the
379 rotation radiograph look like arrays located above and below the rows of basic reflections.
380 Analysis of the diffraction pattern showed that the distribution scheme of satellites characterizing
381 the sample was the same as for previously studied lazurites from the Baikal Lake area and
382 Southwestern Pamir (Sapozhnikov 1992). The difference was in the magnitude of the structure
383 modulation parameter, which was determined by the satellite displacement from the basic
384 reflections along the reciprocal lattice axis. The parameter n was determined from the lazurite
385 single-crystal X-ray rotation photograph (Fig. 8) and refined using the symmetric satellites at the
386 strong basic lines 211, 222, and 411 in the powder diffraction pattern (Table 5) using the
387 following expressions:

388 $$n = \frac{a^2}{12}\left(\frac{1}{d^2_{2+n,1+n,1}} - \frac{1}{d^2_{2-n,1-n,1}}\right),\ n = \frac{a^2}{8}\left(\frac{1}{d^2_{2,1+n,1+n}} - \frac{1}{d^2_{2,1-n,1-n}}\right),$$

389 $$n = \frac{a^2}{16}\left(\frac{1}{d^2_{2+n,2+n,2}} - \frac{1}{d^2_{2-n,2-n,2}}\right), \text{ and } n = \frac{a^2}{12}\left(\frac{1}{d^2_{4+n,1-n,1}} - \frac{1}{d^2_{4-n,1+n,1}}\right).$$

390 The refined n value of 0.1479 was put into quadratic form for cubic crystals

391 $$\frac{1}{d_s^2} = \frac{(h \pm n)^2 + (k \pm n)^2 + l^2}{a^2},$$

392 where d_s is the interplanar spacing of a satellite, a is the basic sub-cell parameter, and hkl are the
393 indices of the main sub-cell reflection near which the satellite under consideration was located.

After that, we determined the d-spacings of other satellites using the exhaustive search and Microsoft Excel software.

Half of the total number of lines in Table 5 correspond to incommensurate satellites. The low value of the reliability index $R = (\Sigma|d_{meas} - d_{calc}|)P^{-1} = 0.002$ Å (where P is the total number of satellites) shows the invariability of the incommensurate displacement of all satellites from the basic reflections. After annealing the mineral in air at 750 °C, the modulation disappeared and the sub-cell parameter increased to 9.107(3) Å. The parameter was estimated from the powder X-ray diffraction pattern of the sample cooled to room temperature, after sample repacking.

Figure 9 shows the dependence of the sub-cell parameter on the annealing temperature in air. The graphs reflect the change in the coefficient of thermal expansion (compression) of lazurite during annealing and cooling. In the range of 30 to 550 °C, the coefficient of thermal expansion $\alpha_1 = 1.87 \cdot 10^{-5}$ K^{-1}. In the interval 550–600 °C, it decreased to near zero ($\alpha_2 = 7.19 \cdot 10^{-7}$ K^{-1}). It should be noted that according to IR spectroscopy data, the interval 550–600 °C corresponds to the completion of water release during heating. In the range of 600 to 750 °C, the mineral begins to expand again, but to a lesser extent than the first time, and $\alpha_3 = 5.54 \cdot 10^{-6}$ K^{-1}.

The irregular change in the sub-cell parameter indicates a change in the thermal expansion mechanism. In the first stage, the expansion proceeds through a simultaneous unfolding of the AlO_4 and SiO_4 tetrahedra according to the mechanism proposed by Pauling (1930) for sodalite. Thermal expansion above 600 °C is caused by a small change in the average distance between the atoms in the framework as the kinetic energy increased. The mismatch in the sub-cell parameters of the initial and annealed mineral at 30 ºC (hysteresis) may be due to partial oxidation of sulfide sulfur under annealing. The parameter of the sub-cell (a), the modulation parameter (n), and the period of incommensurate modulation of the structure (T_m) are related by the equation $a = nT_m$. In the studied mineral, the period of incommensurate modulation equalled 61.82 Å. In the structure of the common cubic lazurite (a = 9.071 Å and n =

419 0.218) from the Baikal Lake area, it equals 41.61 Å (Ivanov and Sapozhnikov 1985; Tauson et
420 al. 1998).

421 **X-ray photoelectron spectroscopy**

422 Figure 10 shows the X-ray photoelectron spectrum of the high-S lazurite sample 1. The
423 BEs and concentration of S-bearing groups are presented in Table 6.

424 Table 6. XPS Data of the S 2p of dark blue lazurite from the Malo-Bystrinskoe deposit.

Photoelectron peak	Binding energy (eV)	FWHM (eV)[a]	MPE[b]	MF[c]
S 2p$_{3/2}$ **S 2p$_{1/2}$**	163.39 164.58	3.6 3.6	$(S_3)^-$	0.26
S 2p$_{3/2}$ **S 2p$_{1/2}$**	168.27 169.45	2.5 2.5	$(SO_4)^{2-}$	0.74

425 [a] Full width at half maximum of peak height
426 [b] Most probable sulfur entities (MPE) from BE values
427 [c] Mole fraction (MF) calculated from the areas of doublets
428
429 Two sulfur species—sulfate sulfur and polysulfide sulfur, were detected by means of
430 XPS. The mole ratio of $(S_3)^-$ to $(SO_4)^{2-}$ was 0.35, which is somewhat lower as compared to the
431 previously calculated value of 0.5 (Table 2). The possible cause of this discrepancy is partial
432 oxidation of sulfur during sample preparation. Nevertheless, the data obtained support the idea
433 that lazurite, being a mineral containing the trisulfide radical anion $(S_3)^-$, was detected in the
434 XPS spectrum as the only polysulfide species incorporated into the structure of high-S lazurite
435 together with sulfate anions. The monosulfide anion S^{2-} was not detected in the S 2p spectrum
436 because of its low content (Table 3) and easy oxidation in powdered form when used for XPS
437 (Tauson et al. 2012).
438 Based on the combination of chemical, IR, Raman, EPR, and XPS data, the charge-
439 balanced empirical formulas calculated on 12 (Al+Si) atoms per formula unit can be written as

440 follows: $(Na_{6.97}Ca_{0.88}K_{0.10})_{\Sigma 7.96}[(Al_{5.96}Si_{6.04})_{\Sigma 12}O_{24}](SO_4)^{2-}_{1.09}(S_3^-)_{0.55}S^{2-}_{0.05}Cl_{0.04}\cdot 0.72H_2O$

441 (sample 1) and

442 $(Na_{7.12}Ca_{0.85}K_{0.01})_{\Sigma 7.97}[(Al_{5.99}Si_{6.01})_{\Sigma 12}O_{24}][(SO_4^{2-},S^{2-})_{1.01}(S_3^-)_{0.82}Cl_{0.02}\cdot nH_2O$ (sample 2). Thus,
443 the idealized formula of S-rich lazurite is $Na_7Ca[Al_6Si_6O_{24}](SO_4)^{2-}(S_3)^-\cdot nH_2O$. It refers to two
444 types of clusters - $[Na_3Ca\cdot SO_4]^{3+}$ and $[Na_4(S_3)^-]^{3+}$, which occupy structural cages in equal
445 proportion.
446

447 ## IMPLICATIONS

448 The ideal crystal-chemical formula of lazurite $Na_6Ca_2[Al_6Si_6O_{24}]S_2$, as recommended in
449 the IMA list of minerals (see Introduction), differs from the ideal formula of lazurite obtained in
450 this work. The difference is of principal value. The "ideal" formula suggests only one kind of
451 sulfur species and one position of sulfur in the lazurite structure. However, it is obvious from
452 chemical and spectroscopic investigation that two different types of sulfur coexist in two
453 different cage sites in the lazurite structure. The formula $Na_7Ca[Al_6Si_6O_{24}]SO_4(S_3)^-\cdot H_2O$,
454 proposed in the present work, is preferable for lazurite because it accounts for the mandatory
455 presence of a voluminous sulfate group in lazurite structural cages, without which the unit cell
456 parameter would be as low as in S-sodalite (i.e., less than 9 Å). It explains the excess of sulfide
457 sulfur atoms as compared to the idealized formula given in the IMA list, and it determines the
458 dark blue "velvet" color of the mineral by the presence of trisulfide radical ion $(S_3)^-$ as a species-
459 defining component.

460 The important conclusion following from the results of investigation of S-rich lazurite is
461 the possibility of the incorporation of the radical ion $(S_3)^-$ into the sodalite β-cage of the lazurite
462 structure. This conclusion, drawn on the basis of chemical data and charge-balance requirement,
463 was confirmed by IR, Raman, EPR, and XPS data. This ubiquitous anion is known to be
464 sufficiently stable under elevated *T* and *P* parameters and different environmental conditions
465 (Chivers and Elder 2013).

Lazurite, the clathrate-type mineral containing constitutional trisulfide radical anions, may be an effective $(S_3)^-$ sensor due to its stability in isolated cages of the lazurite structure. This may be important because of the predicted high complexation ability of $(S_3)^-$ with heavy and precious metals in hydrothermal solutions (Pokrovski et al. 2015). On the other hand, the matrix isolation phenomenon enabled us to study the behavior of this radical anion over much larger ranges of *T* and *P* than would be possible for free species.

Another implication concerns evaluation of redox conditions of the metasomatic processes. It is highly likely that the $(SO_4)^-/(S_3)^-$ ratio depends on oxygen and sulfur dioxide fugacities during lazurite formation (Tauson et al. 2011).

The provenance of lapis lazuli used in antiquity is determined by so-called "strong markers," mainly based on the type and composition of coexisting minerals in the lazurite-containing rocks (Lo Giudice et al. 2017). A distinctive feature of numerous lazurite samples from deposits in the Baikal Lake area is the presence of specific types of incommensurate structure modulation, the common one being 41.6 Å, whereas the 61.8 Å modulation described in this paper for high-S lazurite is rare. An additional point is that the types and ratios of cage clusters may be important geochemical markers.

ACKNOWLEDGMENTS

The research was performed within the framework of state task IX.124.3, registration No. AAAA-A17-117041910035-2. The IR spectroscopy study was partly performed in accordance with state task, registration No. AAAA-A19-119092390076-7. The Raman spectroscopy study was supported by the Russian Foundation for Basic Research, grant no. 18-29-12007. The study of dehydration of samples was carried out with the support of the grant RSF 18-72-10085. The authors would like to thank anonymous reviewers and Prof. Andrey G. Bulakh for constructive criticism and useful comments.

REFERENCES CITED

Arieli D, Vaughan DEW, Goldfarb D (2004) New synthesis and insight into the structure of blue ultramarine pigments. J Am Chem Soc 126: 5776–5788. https://doi.org/10.1021/ja0320121

Balassone G, Bellatreccia F, Mormone A, Biagioni C, Pasero M, Petti C, Mondillo N, Fameli G (2012) Sodalite-group minerals from the Somma-Vesuvius volcanic complex, Italy: a case study of K-feldspar-rich xenoliths. Min Mag 76(1):191–212.

Bellatreccia F, Della Ventura G, Piccinini M, Cavallo A, Brilli M (2009) H_2O and CO_2 in minerals of the hauyne-sodalite group: an FTIR spectroscopy study. Miner Mag 73: 399–413. https://doi.org/10.1180/minmag.2009.073.3.399

Belov NV (1976) Essays on structural mineralogy. Nedra, Moscow (in Russ.).

Bolotina NB (2006) Isotropic lazurite: A cubic single crystal with an incommensurate three-dimensional modulation of the structure. Crystallogr Rep 51:968–976. https://doi.org/10.1134/S106377450606006X

Chivers T, Elder PJW (2013) Ubiquitous trisulfur radical anion: fundamentals and applications in materials science, electrochemistry, analytical chemistry and geochemistry. Chem Soc Rev 42:5996–6005. https://doi.org/10.1039/c3cs60119f

Clark RJH, Cobbold DG (1978) Characterization of sulfur radical-ions in solutions of alkalipolysulfides in dimethylformamide and hexamethylphosphoramide and in solid-state in ultramarine blue, green, and red. Inorg Chem 17: 3169–3174. https://doi.org/10.1021/ic50189a042

Clark RJH, Dines TJ, Kurmoo M (1983) On the nature of the sulfur chromophores in ultramarine blue, green, violet, and pink and of the selenium chromophore in ultramarine selenium – characterization of radical-ions by electronic and resonance Raman spectroscopy and the determination of their excited-state geometries. Inorg Chem 22: 2766–2772. https://doi.org/10.1021/ic00161a024

Climent-Pascual E, de Paz JR, Rodríguez-Carvajal E, Suard E, Sáez-Puche R (2009) Synthesis and characterization of the ultramarine-type analog $Na_{8-x}[Si_6Al_6O_{24}]\cdot(S^{-2},S^{-3},CO_3)_{(1-2)}$. Inorg Chem 48:6526–6533. https://doi.org/10.1021/ic900438c

Deer WA, Howie RA, Wise WS, Zussman J (2004) Rock-forming minerals. Volume 4B. Framework silicates: silica minerals. Feldspathoids and the zeolites. The Geological Society, London.

Evsyunin VG, Rastsvetaeva RK, Sapozhnikov AN, Kashaev AA (1998) Modulated structure of orthorhombic lazurite. Crystallogr Rep 43:999–1002. http://dx.doi.org/10.1134/1.170884

Evsyunin VG, Sapozhnikov AN, Kashaev AA, Rastsvetaeva RK (1997) Crystal Structure of Triclinic Lazurite. Crystallogr Rep 42:938–945. https://dx.doi.org/10.1134/1.170716

Fechtelkord M (1999) Structural study of $Na_8[AlSiO_4]_6(CO_3)_x(HCOO)_{2-2x}(H_2O)_{4x}$, $0.2 \leq x \leq 1$, synthesized in organic solvents: order and disorder of carbonate and formate anions in sodalite. Micropor Mesopor Mater 28:335–351. https://doi.org/10.1016/S1387-1811(98)00302-3

Fleet ME, Liu X, Harmer SL, Nesbitt HW (2005) Chemical state of sulfur in natural and synthetic lazurite by SK-edge xanes and X-ray photoelectron spectroscopy. Can Miner 43:1589–1603. https://doi.org/10.2113/gscanmin.43.5.1589

Forbes TZ, Radha AV, Navrotsky A (2011) The energetics of nanophase calcite. Geochim Cosmochim Acta 75:7893–7905. https://doi.org/10.1016/j.gca.2011.09.034

Gadiyatov V (2012) Gems – the stone rainbow of Earth. Voronezh State University, Voronezh. (in Russ.).

Gesing TM, Buhl JC (1998) Crystal structure of a carbonate-nosean $Na_8[AlSiO_4]_6CO_3$. Eur J Miner 10:71–77. https://doi.org/10.1127/ejm/10/1/0071

Gobeltz-Hautecoeur N, Demortier A, Lede B, Lelieur JP, Duhayon C (2002) Occupancy of the sodalite cages in the blue ultramarine pigments. Inorg Chem 41:2848–2854. https://doi.org/10.1021/ic010822c

Nassan I, Busek PR (1989) Incommensurate-modulated structure of nosean, a sodalite-group mineral. Amer Miner 74:394–410.

Hassan I, Grundy HD (1984) The crystal structures of sodalite-group minerals. Acta Cryst B 40:6–13. https://doi.org/10.1107/S0108768184001683

Hassan I, Grundy HD (1989) The structure of nosean, ideally $Na_8[Al_6Si_6O_{24}]SO_4 \cdot H_2O$. Can Miner 27:165–172.

Hassan I, Grundy HD (1991) The crystal structure of basic cancrinite, ideally $Na_8[Al_6Si_6O_{24}](OH)_2 \cdot 3H_2O$. Can Miner 29:123–130.

Hassan I, Peterson RC, Grundy HD (1985) The structure of lazurite, ideally $Na_6Ca_2(Al_6Si_6O_{24})S_2$, a member of the sodalite group. Acta Cryst C 41:827–832. https://doi.org/10.1107/S0108270185005662

Hogarth DD, Griffin WL (1976) New data on lazurite. Lithos 9:39–54. https://doi.org/10.1016/0024-4937(76)90055-4

Ivanov VG, Sapozhnikov AN (1985) Lazurites of the USSR. Nauka, Novosibirsk. (in Russ.)

Li S, Liu M, Sun L (2011) Preparation of acid-resisting ultramarine blue by novel two-step silica coating process. Indust Eng Chem Res 50:7326–7331. https://doi.org/10.1021/ie200343k

Lo Giudice A, Angelici D, Re A, Gariani G, Borghi A, Calusi S, Giuntini L, Massi M, Castelli L, Taccetti F, Calligaro T, Pacheco C, Lemasson Q, Pichon L, Moignard B, Pratesi G, Guidotti MC (2017). Protocol for lapis lazuli provenance determination: evidence for an Afghan origin of the stones used for ancient carved artefacts kept at the Egyptian Museum of Florence (Italy). Archaeol Anthropol Sci 9:637–651. https://doi.org/10.1007/s12520-016-0430-0

Ostroumov M, Fritsch E, Faulques E, Chauvet O (2002) Etude spectrometrique de la lazurite du Pamir, Tajikistan. Can Miner 40: 885-893. https://doi.org/ 10.2113/gscanmin.40.3.885

Pauling L (1930) The structures of sodalite and helvite. Z Kristallogr 74:213–225.

Pinon V, Levillain E, Lelieur J (1992) The S_3^- radical as a standard for ESR experiments. J Magn Res 96:31–39. https://doi.org/10.1016/0022-2364(92)90285-F

Platonov AN, Tarashchan AN, Belichenko VP, Povarennikh AS (1971) Spectroscopic study of sulfide sulfur in some framework aluminosilicates. Constitution and Properties of Minerals 5: 61–72 (in Russ.).

Pokrovski GS, Kokh MA, Guillaume D, Borisova AY, Gisquet P, Hazemann J-L, Lahera E, Net WD, Proux O, Testemale D, Haigis V, Jonchiere R, Seitsonen AP, Ferlat G, Vuilleumier R, Saitta AM, Boiron M-C, Dubessy J (2015) Sulfur radical species form gold deposits on Earth. PNAS 112:13484–13489. www.pnas.org/cgi/doi/10.1073/pnas.1506378112

Reshetnyak NB, Tretyakova LI, Vokhmentsev A.Y. (1986) Investigation of colour centrums in natural lazurite by means of Raman spectroscopy. Mineralogicheskiy Zhurnal 8(5):49–60 (in Russ.).

Samoilovich MI (1971) An ESR study of sulfur-bearing radical ions in minerals. Geokhimiya 4:477–483 (in Russ.).

Sapozhnikov AN (1992) Modulated structure of lazurite from deposits in southwestern Pamir. Sov Phys Crystallogr 37:470–472.

Sapozhnikov AN, Kaneva EV, Cherepanov DI, Suvorova LF, Ivanova LA, Reznitsky LZ (2012) Vladimirivanovite $Na_6Ca_2[Al_6Si_6O_{24}]$ $(SO_4, S^{-3}, S^{-2}, Cl)_2 \cdot H_2O$, a new mineral of sodalite group. Geol Ore Deposits 54:557-564. https://doi.org/10.1134/S1075701512070070.

Steudel R. (2003) Inorganic polysulfides S_n^{2-} and radical anions $S_n^{\cdot-}$. In: Steudel R (ed.) Elemental Sulfur und Sulfur-Rich Compounds II. Topics in Current Chemistry, vol 231. Springer, Berlin – Heidelberg.

589 Tauson VL, Akimov VV, Sapozhnikov AN, Kuznetzov KE (1998) Investigation of the stability
590 conditions and structural-chemical transformations of Baikal lazurite. Geochem Int
591 36:717–733.
592 Tauson VL, Goettlicher J., Sapozhnikov AN, Mangold S, Lustenberg EE (2012) Sulfur
593 speciation in lazurite-type minerals $(Na,Ca)_8[Al_6Si_6O_{24}](SO_4,S)_2$ and their annealing
594 products: a comparative XPS and XAS study. Eur J Miner 24:133–152.
595 https://doi.org/10.1127/0935-1221/2011/0023-2132
596 Tauson VL, Sapozhnikov AN, Shinkareva SN, Lustenberg EE (2011) Indicative properties of
597 lazurite as a member of clathrasil mineral family. Dokl Earth Sci 441:1732–1737.
598 https://doi.org/10.1134/S1028334X11120312
599 Taylor D (1967) The sodalite group of minerals. Contr Mineral Petrol 16: 172–188.
600 Tossell JA (2012) Calculation of the properties of the S_3^- radical anion and its complexes with
601 Cu^+ in aqueous solution. Geochim Cosmochim Acta 95:79–92.
602 Wells AF (1984) Structural inorganic chemistry. Calderon Press, Oxford.
603 Wong MW (2003) Quantum chemical calculations of sulfur-rich compounds. In: Steudel R (ed.)
604 Elemental sulfur and sulfur-rich compounds II. Springer, p. 143.
605

606 ## FIGURE CAPTIONS

607 Fig. 1. Samples of rocks with high-sulfur lazurite: (*a*) lenticular body (sample 1), (*b)* lazurite-
608 containing calciphyre with bystrite (sample 2). Abbreviations: Lzr-lazurite, Bys-bystrite, Cal-
609 calcite.

610 Fig. 2. Thermogravimetric (TG) and differential scanning calorimetry (DSC) curves and the
611 temperature dependence of the SO_2^- ion current (mass number 64) for lazurite sample 1.

612 Fig. 3. Raman spectrum of S-rich lazurite (sample 1).

613 Fig. 4. Infrared absorption spectrum of S-rich lazurite (sample 1).

614 Fig. 5. Temperature dependence as a function of relative intensity of IR absorption at 3400 cm^{-1}
615 (stretching vibrations of H_2O molecules).

616 Fig. 6. EPR spectrum of S-rich lazurite at room temperature.

617 Fig. 7. Single-crystal X-ray rotation photographs of lazurite (a = 9.071 Å and n = 0.218): initial
618 crystal of lazurite with (*a*) incommensurate modulation reflections and (*b*) crystal annealed at
619 650 °C in air for 1 hour, without incommensurate modulation reflections.

620 Fig. 8. The [100] single-crystal X-ray rotation photograph of S-rich lazurite (sample 1).
621 Reflections of the subcell (basic), commensurate modulation (com), incommensurate modulation
622 (incom), and β-reflections (β-refl) are indicated.

623 Fig. 9. Dependence of the sub-cell parameter of S-rich lazurite on temperature.

624 Fig. 10. S 2p XPS spectra of the dark blue lazurite from the Malo-Bystrinskoe deposit. The peak
625 parameters are given in Table 6.

626

This is the peer-reviewed, final accepted version for American Mineralogist, published by the Mineralogical Society of America.
The published version is subject to change. Cite as Authors (Year) Title. American Mineralogist, in press.
DOI: https://doi.org/10.2138/am-2020-7317. http://www.minsocam.org/

FIGURES

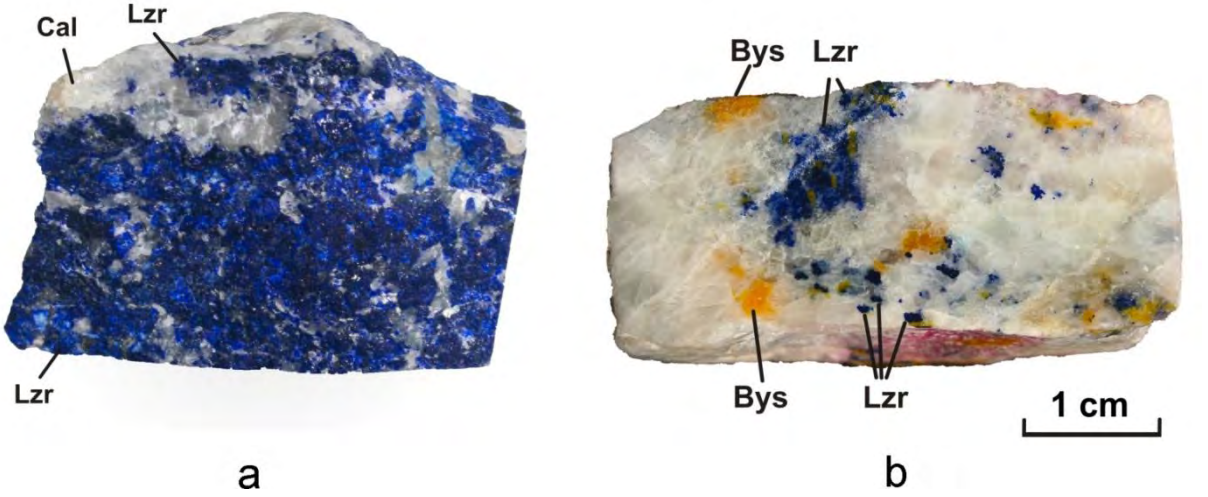

Fig. 1. Samples of rocks with high-sulfur lazurite: *a* – lenticular body (sample 1), *b* – lazurite-containing calciphyre with bystrite (sample 2). Abbreviations: Lzr-lazurite, Bys-bystrite, Cal-calcite .

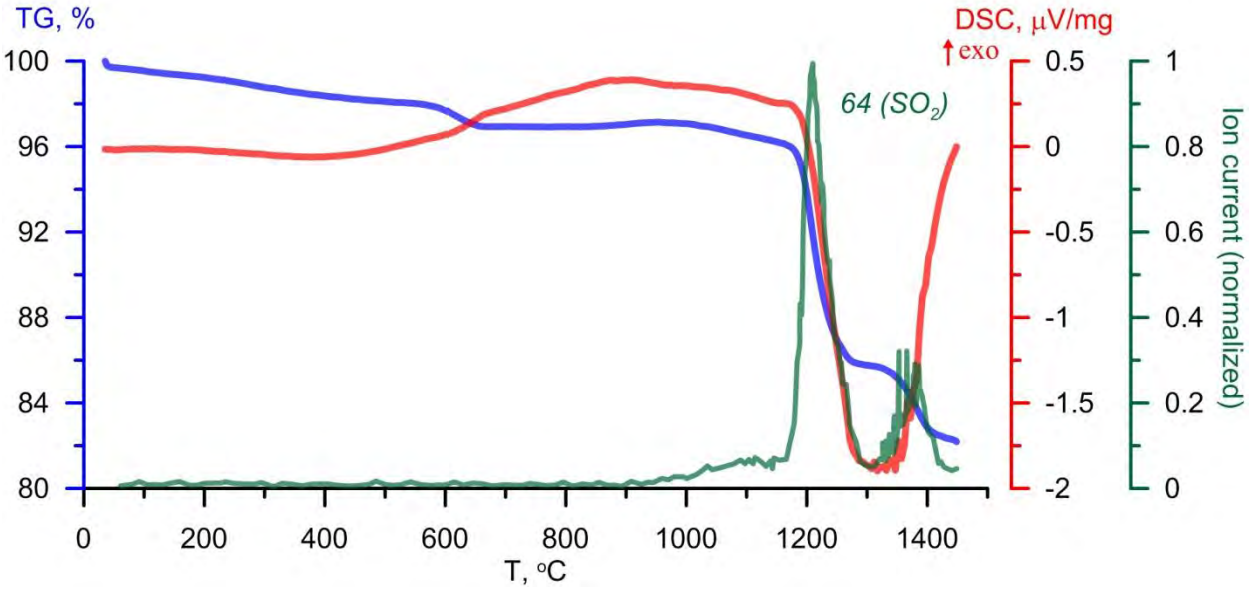

Fig. 2. Thermogravimetric (TG) and differential scanning calorimetry (DSC) curves, and the temperature dependence of the SO_2^- ion current (the mass number of 64) for the lazurite sample. 1.

This is the peer-reviewed, final accepted version for American Mineralogist, published by the Mineralogical Society of America.
The published version is subject to change. Cite as Authors (Year) Title. American Mineralogist, in press.
DOI: https://doi.org/10.2138/am-2020-7317. http://www.minsocam.org/

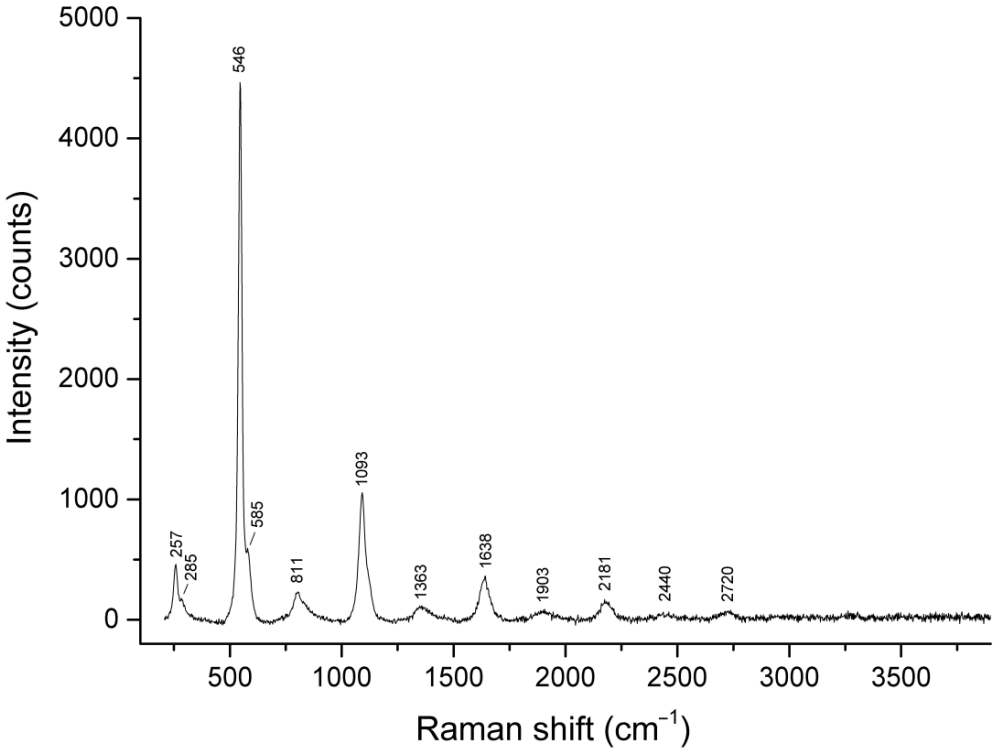

638

639 Fig. 3. Raman spectrum of S-rich lazurite (sample 1).

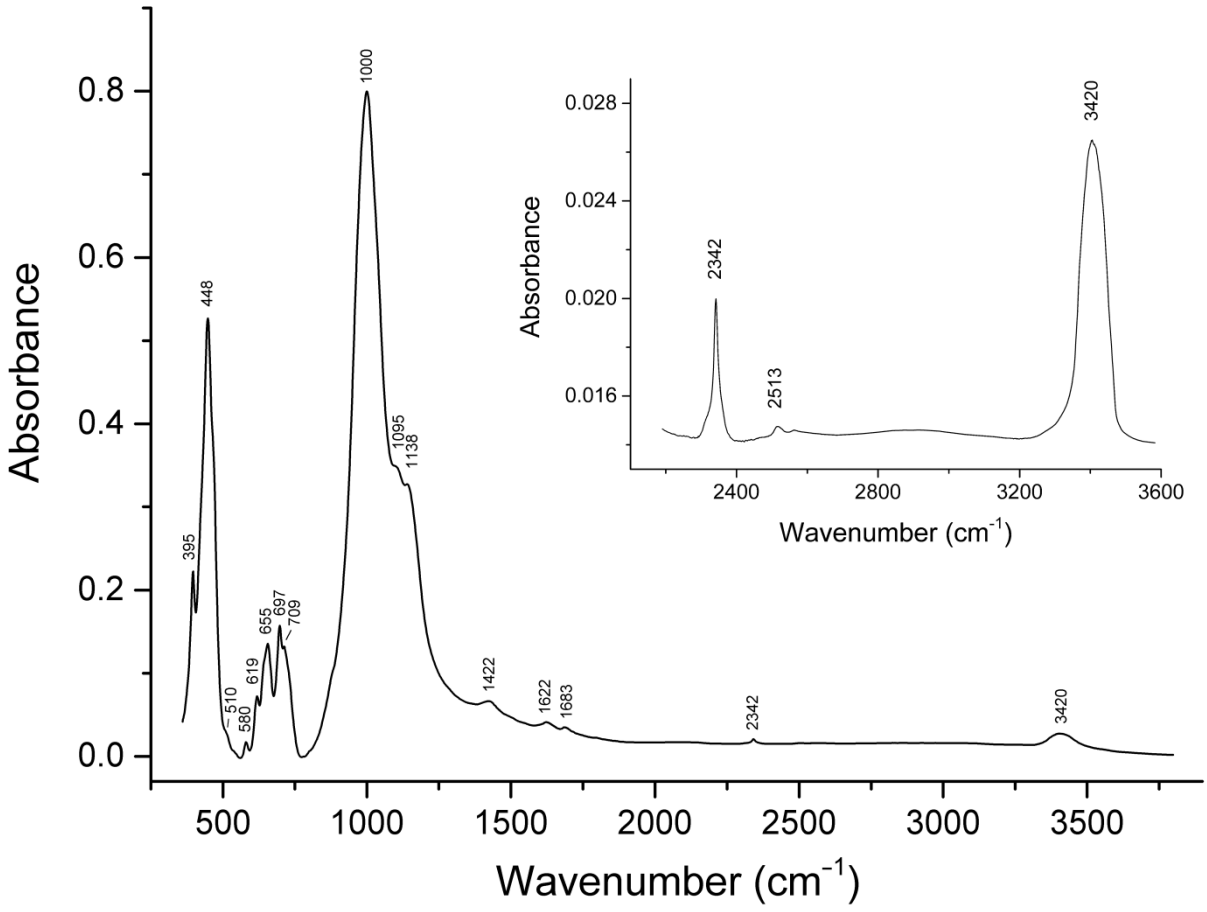

640

641 Fig. 4. Infrared absorption spectrum of S-rich lazurite (sample 1).

This is the peer-reviewed, final accepted version for American Mineralogist, published by the Mineralogical Society of America.
The published version is subject to change. Cite as Authors (Year) Title. American Mineralogist, in press.
DOI: https://doi.org/10.2138/am-2020-7317. http://www.minsocam.org/

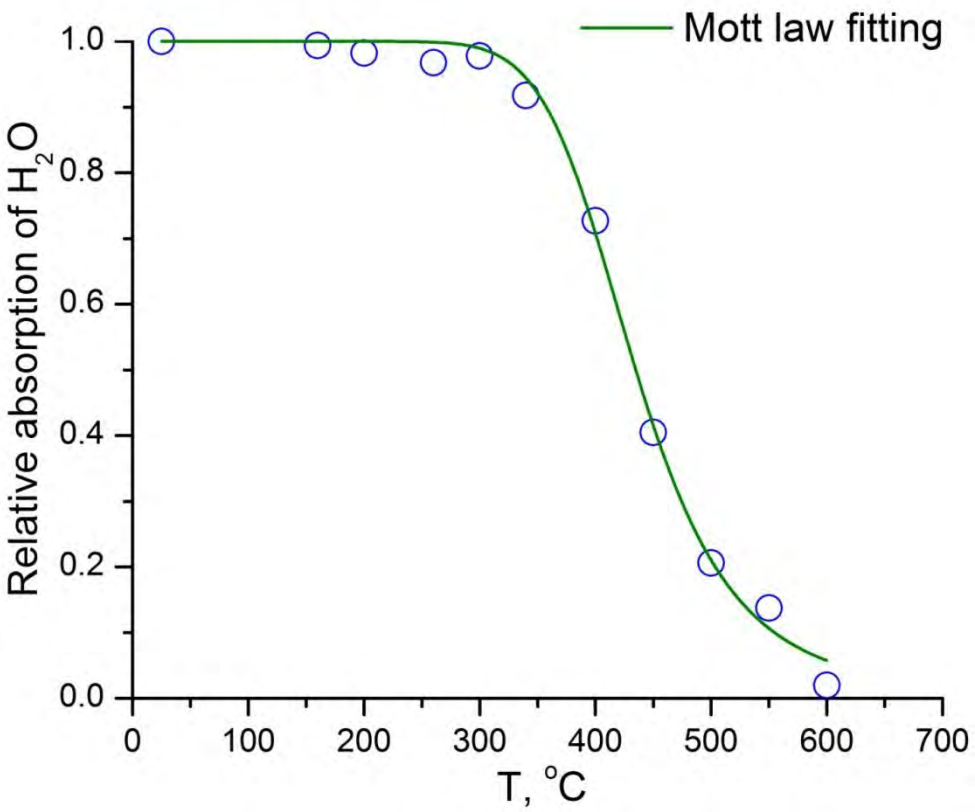

Fig. 5. Temperature dependence of relative intensity of IR absorption at 3400 cm^{-1} (stretching vibrations of H_2O molecules).

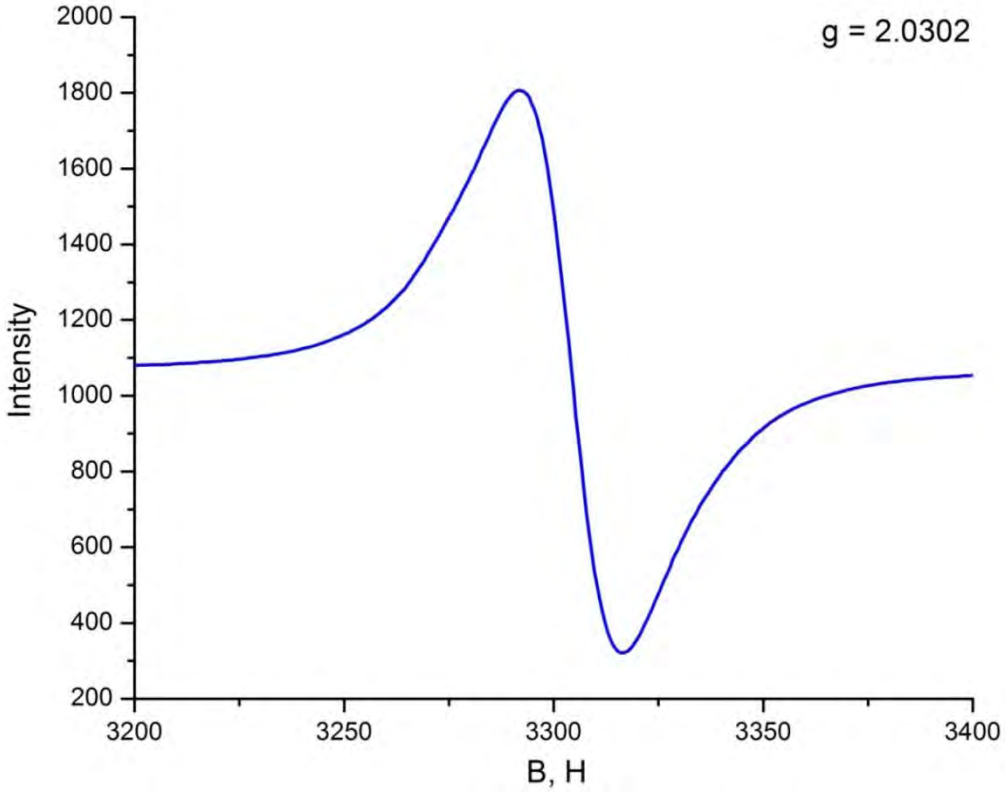

Fig. 6. The EPR spectrum of S-rich lazurite at room temperature.

This is the peer-reviewed, final accepted version for American Mineralogist, published by the Mineralogical Society of America.
The published version is subject to change. Cite as Authors (Year) Title. American Mineralogist, in press.
DOI: https://doi.org/10.2138/am-2020-7317. http://www.minsocam.org/

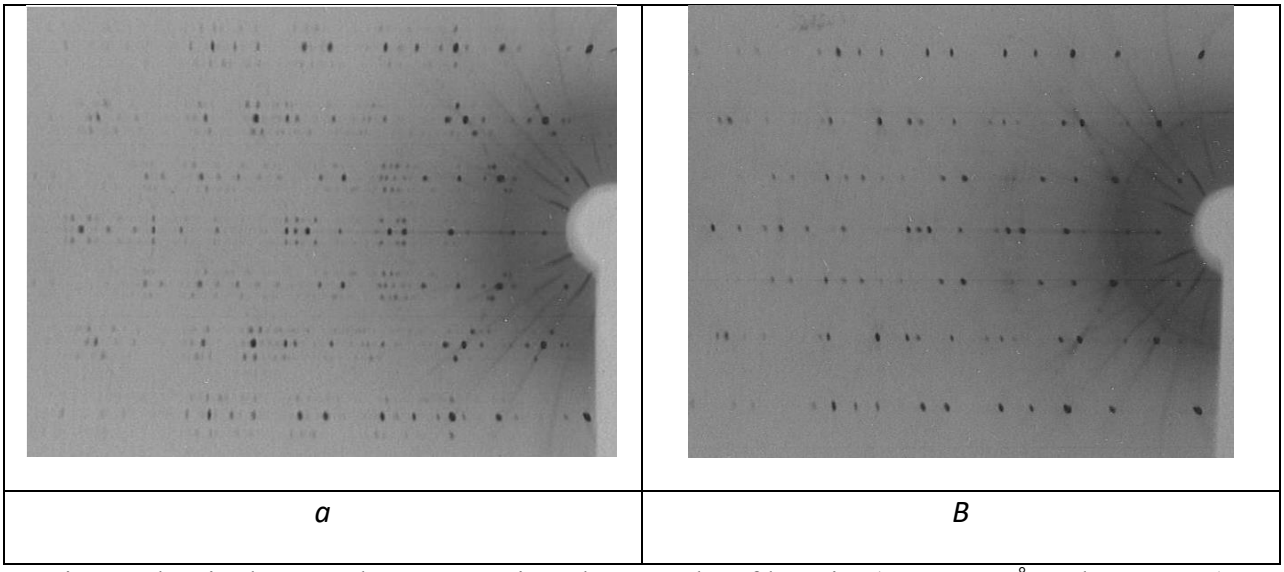

Fig. 7. The single-crystal X-ray rotation photographs of lazurite (a = 9.071 Å and n = 0.218): initial crystal of lazurite with incommensurate modulation reflections (a) and crystal annealed at 650° in air during 1 hour, without incommensurate modulation reflections (b).

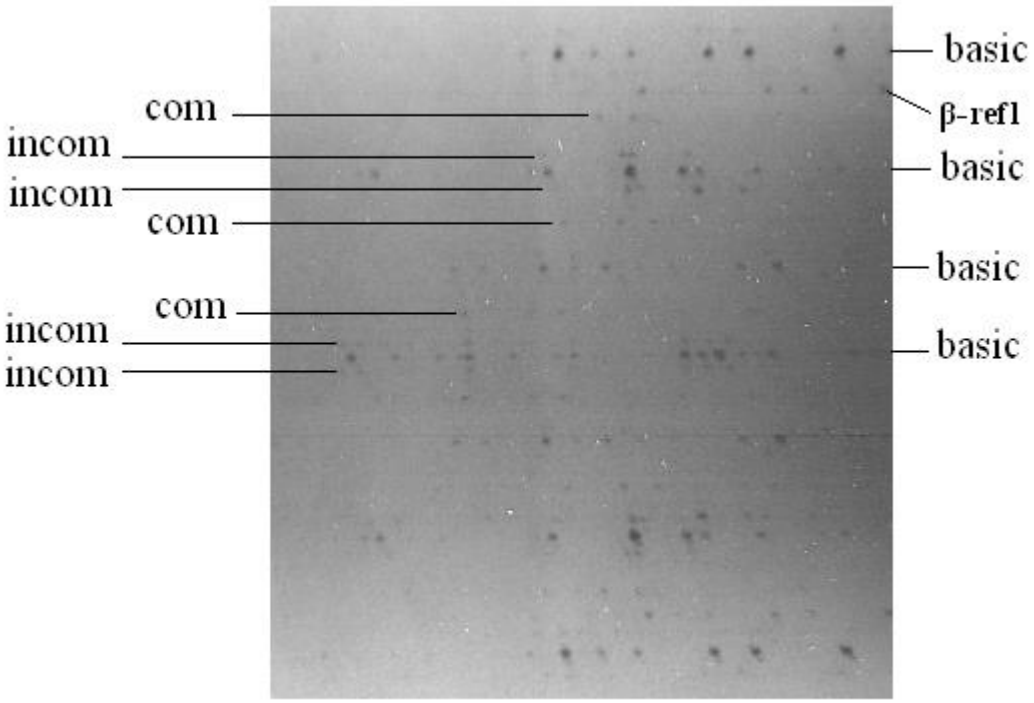

Fig. 8. The [100] single-crystal X-ray rotation photograph of S-rich lazurite (sample 1). Reflections of the subcell (basic), commensurate modulation (com), incommensurate modulation (incom) and β-reflections (β-refl) are indicated.

This is the peer-reviewed, final accepted version for American Mineralogist, published by the Mineralogical Society of America.
The published version is subject to change. Cite as Authors (Year) Title. American Mineralogist, in press.
DOI: https://doi.org/10.2138/am-2020-7317. http://www.minsocam.org/

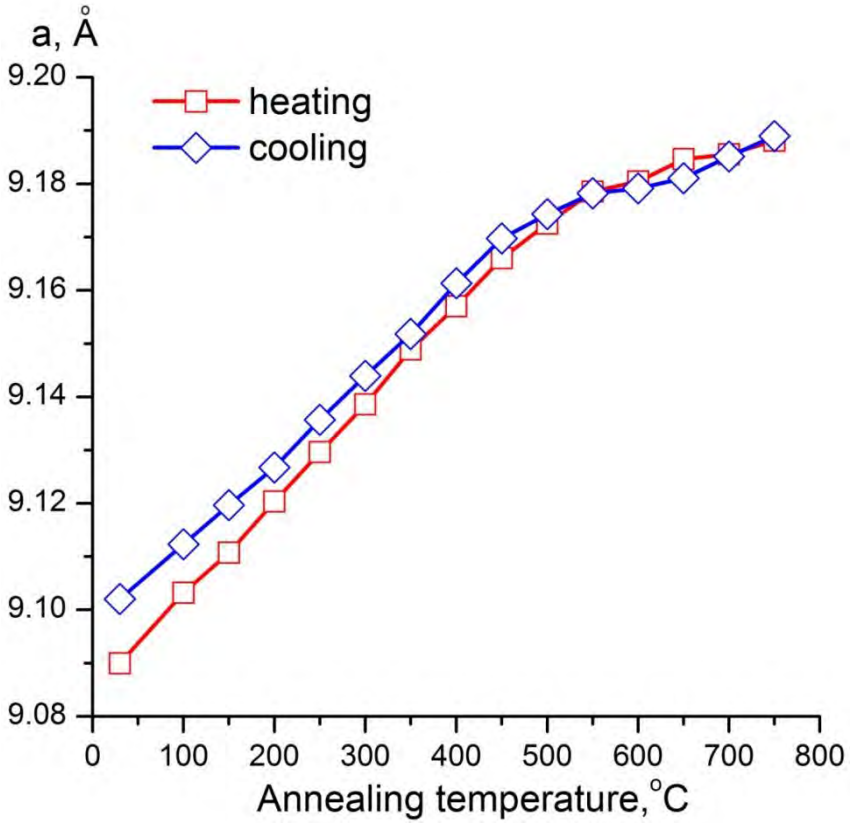

Fig. 9. The dependence of the sub-cell parameter of S-rich lazurite on temperature.

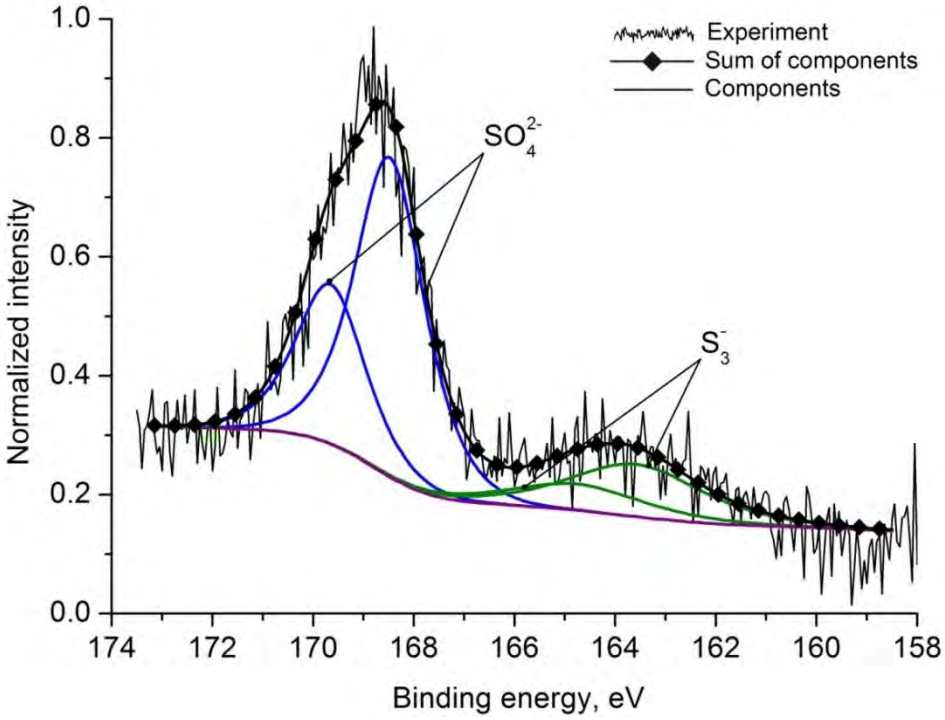

Fig. 10. S 2p XPS spectra of the dark blue lazurite from the Malo-Bystrinskoe deposit. The peak parameters are shown in Table 6.